

# FaithDiff: Unleashing Diffusion Priors for Faithful Image Super-resolution

Junyang Chen Jinshan Pan Jiangxin Dong<sup>†</sup>

School of Computer Science and Engineering, Nanjing University of Science and Technology

[https://jychen9811.github.io/FaithDiff\\_page/](https://jychen9811.github.io/FaithDiff_page/)

## Abstract

*Faithful image super-resolution (SR) not only needs to recover images that appear realistic, similar to image generation tasks, but also requires that the restored images maintain fidelity and structural consistency with the input. To this end, we propose a simple and effective method, named FaithDiff, to fully harness the impressive power of latent diffusion models (LDMs) for faithful image SR. In contrast to existing diffusion-based SR methods that freeze the diffusion model pre-trained on high-quality images, we propose to unleash the diffusion prior to identify useful information and recover faithful structures. As there exists a significant gap between the features of degraded inputs and the noisy latent from the diffusion model, we then develop an effective alignment module to explore useful features from degraded inputs to align well with the diffusion process. Considering the indispensable roles and interplay of the encoder and diffusion model in LDMs, we jointly fine-tune them in a unified optimization framework, facilitating the encoder to extract useful features that coincide with diffusion process. Extensive experimental results demonstrate that FaithDiff outperforms state-of-the-art methods, providing high-quality and faithful SR results.*

## 1. Introduction

Image super-resolution (SR) aims to recover high-quality (HQ) images from low-quality (LQ) ones with unknown degradations. This problem has attracted widespread attention and achieved significant progress due to the development of deep learning methods. However, it is still challenging to restore faithful SR images with high reality and fidelity, owing to the ill-posed property of SR problems.

Most state-of-the-art image SR methods rely on deep generative models, which aim to learn the distribution of HQ images and recover vivid textures from LQ inputs. Generative Adversarial Networks (GANs), as one of the representative approaches, can recover sharp images with rich

details [3, 4, 39, 40, 46]. However, the training process of GAN-based methods is unstable and the generated images usually exhibit perceptually unpleasant artifacts as pointed out by [4, 19, 42]. To alleviate these issues, several methods [4, 49] propose to construct a discrete codebook consisting of a pre-defined number of HQ feature vectors and learn to match LQ features to a set of HQ ones, which have achieved better perceptual quality. Nevertheless, due to the vastness of the natural image space, priors encoded with a fixed size of codebook inherently possess a limited ability of representation, hindering faithful image SR results.

Recently, latent diffusion models (LDMs) [5, 26, 31, 32] have achieved promising image generation results as they can effectively model complex image distributions. While LDMs possess strong priors on the structures and details of HQ images, they face challenges in the image SR task, which requires not only vivid generation details but also faithful structure recovery that is consistent with LQ inputs. To address this, several methods [21, 27, 43, 44] enhance the encoder to extract degradation-robust features from LQ images and then leverage pre-trained diffusion models to refine the extracted features. However, real-world images with unknown degradations present challenges for the encoder in extracting features with faithful structural information. As the diffusion models are pre-trained on HQ images, any mistakes in the extracted features (Figure 1(b)-(c)) may be misinterpreted by the diffusion model as image structures, thus misleading the diffusion process and negatively impacting the final restoration results (*e.g.*, the characters) in Figure 1(d) and (f)-(g). As a result, relying solely on improving the extracted features for guiding the diffusion process has limitations in achieving faithful restoration. Different from the above methods, we unleash and fine-tune the diffusion model to identify useful information from degraded inputs and boost faithful image SR.

Note that the encoder and the diffusion model play different but indispensable roles in LDM-based SR methods [21, 44]. Separately optimizing these two modules will limit the power of LDMs, hindering the restoration of fine-scale structures as analyzed in Section 5. Thus, we propose to jointly optimize the encoder and diffusion model, estab-

<sup>†</sup>Corresponding author

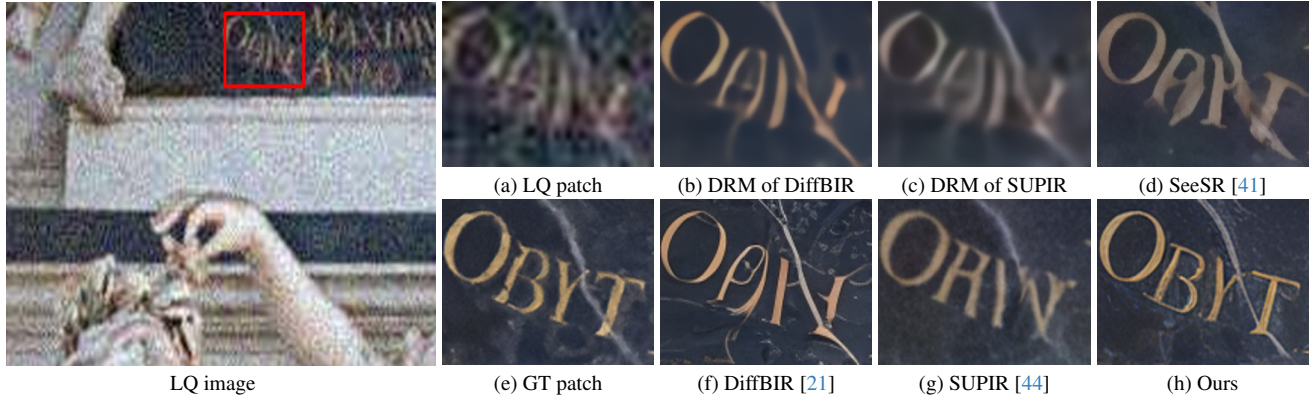


Figure 1. Visual comparison with state-of-the-art SR methods. (b) and (c) are the intermediate results of the degradation removal module (DRM) by DiffBIR [21] and SUPIR [44]. The competing methods [21, 44] do not effectively restore faithful structures based on the degradation removal results in (b)-(c). In contrast to the results in (d) and (f)-(g), our approach can recover more realistic high-quality results with faithful contents (*e.g.*, the characters in (h)).

lishing a more powerful LDM for image SR. In addition, we develop a simple alignment module to help the encoder align well with the progressive diffusion process. In this way, the encoder is able to provide useful latent features that coincide with the diffusion process and the diffusion model can further restore the features for better reconstruction. Benefited from their interplay, the proposed method is able to distinguish between degradation effects and inherent structural information, and recover high-quality and faithful results, as shown in Figure 1(h).

The contributions of this work are summarized as follows: (i) We propose an effective method, named FaithDiff, which unleashes diffusion priors to better harness the powerful representation ability of LDM for image SR. A detailed analysis demonstrates that unleashing diffusion priors is more effective in exploring useful information from degraded inputs, suppressing reconstruction errors, and recovering faithful structures. (ii) We develop a simple yet effective alignment module to align the latent representation of LQ inputs, encoded by the encoder, with the noisy latent of the diffusion model. (iii) We jointly fine-tune the encoder and the diffusion model to benefit from their interplay. (iv) We quantitatively and qualitatively demonstrate that our FaithDiff performs favorably against state-of-the-art methods on both synthetic and real-world benchmarks.

## 2. Related Work

**Image super-resolution.** Image SR is a highly ill-posed problem, and early approaches [6, 11, 45] focus primarily on developing methods to estimate degradation kernels for restoration. However, due to the complexity of degradation in real-world scenarios, these methods often fail to remove degradation artifacts and recover sharp edges effectively. To better solve real-world degradation effects, Zhang et al. [40] and Wang et al. [46] consider more complex degradation

scenarios and propose high-order degradation models to address real-world degradations.

By incorporating high-order degradation models, several GAN-based methods [4, 18, 40, 46] provide promising visual results. However, GAN-based approaches often suffer from perceptually unpleasant artifacts. Liang et al. [19] and Xie et al. [42] attempt to mitigate this issue by penalizing regions with such artifacts. Nonetheless, these methods still struggle to recover fine details in LQ images.

With the success of generative large models such as Stable Diffusion [26, 31], several recent methods leverage generative priors to solve image SR problem [21, 27, 38, 41, 43, 44]. Yang et al. [43] introduce a degradation removal module that extracts degradation-insensitive features from LQ images to guide the diffusion process for restoration. Lin et al. [21] explicitly divide the restoration process into two stages: degradation removal and detail regeneration. It first uses MSE-based restoration models to achieve degradation removal and then employs generative priors for detail enhancement. Yu et al. [44] also adopt a similar two-stage restoration approach. Although promising results have been achieved, the performance of these algorithms is limited by the accuracy of degradation removal results.

**Diffusion model.** Recently, Denoising Diffusion Probabilistic Models (DDPM) [9] demonstrate remarkable capabilities in generating high-quality natural images. Rombach et al. [31] extend the DDPM framework to the latent space, achieving impressive results in text-to-image synthesis. This advancement leads to the proliferation of large pre-trained text-to-image diffusion models, such as Stable Diffusion (SD) [31], Imagen [32], and PixelArt- $\alpha$  [5]. Several studies [29, 30] show that text-to-image diffusion priors are more effective than GAN priors in handling diverse natural images. Lv et al. [47] and Mou et al. [25] use edge maps, segmentation maps, etc., as additional inputs to better control the diffusion process to generate specified content.

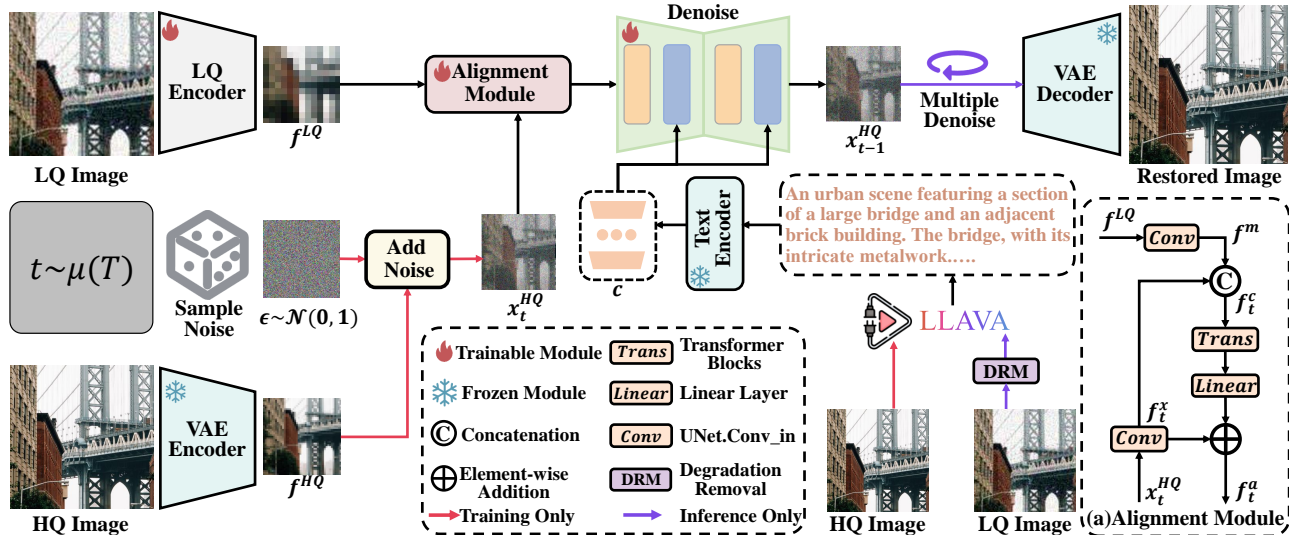


Figure 2. **An overview of the FaithDiff**, which takes LQ images and image descriptions as inputs and restores HQ images via diffusion process. To fully leverage the power of LDMs, we propose to unleash diffusion priors. An alignment module is developed to effectively incorporate the features extracted from LQ images with the noisy latent of the diffusion model. We jointly optimize the encoder, the alignment module, and the diffusion model, which can benefit from their interplay and lead to faithful SR images with high visual quality.

Hu et al. [10] and Tian et al. [34] achieve promising results in human pose deformation and facial animation by leveraging pre-trained diffusion models. While these methods generate visually diverse output, they face challenges in image SR task, which require recovering faithful structural details from LQ images.

### 3. FaithDiff

Our goal is to present an effective method to fully harness the power of LDM for image SR. Specifically, we first employ the encoder of a pre-trained Variational Autoencoder [15] (VAE) to map LQ inputs into the latent space and extract the corresponding LQ features. Then, we develop an alignment module to effectively transfer useful information from the latent LQ features and ensure them align well with the diffusion process. In addition, we incorporate text embeddings, extracted from image descriptions using a pre-trained text encoder, as auxiliary information. These embeddings are integrated with the latent features of the diffusion model through cross-attention layers to help explore useful structural information. Furthermore, we propose a unified feature optimization strategy to jointly fine-tune the VAE encoder and the diffusion model, allowing the encoder to extract useful information from LQ images that facilitates the diffusion process while enabling the diffusion model to further refine the extracted feature for HQ image SR. Finally, we obtain the restored image from the refined features by a pre-trained VAE decoder. Figure 2 summarizes the network architecture. In the following, we present the details

of the proposed approach.

#### 3.1. LQ feature extraction

Given an LQ image, we extract the LQ features  $f^{LQ}$  through a VAE encoder. Existing methods [21, 44] mostly adopt the features extracted from the last layer of the VAE encoder as the LQ features. However, the last layer of the encoder significantly compresses the channel dimensions of the features (e.g., only 8 channels used in [21, 44]), which is insufficient to capture both the degradation factors and structural details in LQ inputs. To obtain sufficient feature information, we propose to employ the features from the penultimate layer of the encoder as  $f^{LQ}$ , which have 512 channels and contain more useful information that is beneficial for the subsequent diffusion process (as demonstrated in Section 5).

#### 3.2. Alignment module

To effectively transmit the information contained in the extracted LQ features  $f^{LQ}$  to control the generation of the diffusion model, a straightforward solution is to add  $f^{LQ}$  with the noisy latent  $x_t^{HQ}$  of the diffusion model after passing them through convolutional layers, respectively. However, as the diffusion process progresses, the  $x_t^{HQ}$  become increasingly clear, while the  $f^{LQ}$  remain unchanged. Therefore, it is unreasonable to directly combine them, as the degradation factors in  $f^{LQ}$  may continuously interfere with the generation of high-quality  $x_t^{HQ}$ .

To this end, we propose an effective alignment module that extracts useful features from  $f^{LQ}$  to achieve better

alignment with  $x_t^{HQ}$ , thus facilitating the subsequent diffusion process. The architecture of the proposed alignment module is illustrated in Figure 2 (a).

First, we individually employ convolutional operations on the LQ features  $f^{LQ}$  as well as the noisy latent  $x_t^{HQ}$ , and obtain their concatenation result as  $f_t^c$ . Then,  $f_t^c$  is put into a stack of two Transformer blocks [36], which facilitates the interaction between the LQ features  $f^{LQ}$  and the noisy latent  $x_t^{HQ}$ . Finally, we obtain the aligned features  $f_t^a$  as

$$\begin{aligned} f_t^x &= \text{Conv}(x_t^{HQ}), f_t^m = \text{Conv}(f^{LQ}), \\ f_t^c &= \text{Concat}(f_t^x, f_t^m), \\ \text{Trans}(f_t^c) &= \mathcal{T}_2(\mathcal{T}_1(f_t^c)), \\ f_t^a &= \text{Linear}(\text{Trans}(f_t^c) + f_t^x), \end{aligned} \quad (1)$$

where  $\mathcal{T}_i$  ( $i = 1, 2$ ) denotes the transformer block [36],  $\text{Conv}(\cdot)$  denotes the  $3 \times 3$  convolution,  $\text{Linear}(\cdot)$  denotes the fully connected layer, and  $\text{Concat}(\cdot)$  denotes the concatenation operation.

Note that our alignment module is simple yet effective. More advanced architectures can also be considered to align the LQ features with the noisy latent of diffusion model.

During the diffusion process, we also leverage text embeddings as additional auxiliary information to help extract useful information from latent features of the diffusion model. These text embeddings are extracted from image descriptions by a pre-trained text encoder [28]. Similar to [43, 44], we utilize the cross-attention layer to establish interactions between text embeddings and latent features, capturing the text-to-image knowledge inherent in LDM. Overall, given the latent HQ features  $x_t^{HQ}$  and the aligned features  $f_t^a$  at the diffusion step  $t$  as well as the text embeddings  $c$ , we can obtain the latent HQ features at the diffusion step  $t - 1$  as

$$x_{t-1}^{HQ} = \frac{1}{\sqrt{\alpha_t}}(x_t^{HQ} - \frac{1 - \alpha_t}{\sqrt{1 - \bar{\alpha}_t}}\hat{\epsilon}_\theta(f_t^a, c, t)) + \sigma_t z, \quad (2)$$

where  $\hat{\epsilon}_\theta$  denotes the diffusion model,  $z$  is sampled from the standard normal distribution  $\mathcal{N}(0, 1)$ ,  $\alpha_t$  and  $\sigma_t$  are the noisy scheduler terms that control sample quality, and  $\bar{\alpha}_t = \prod_{i=1}^t \alpha_i$ .

### 3.3. Unified feature optimization

Our FaithDiff contains an LQ feature extraction module (*i.e.*, a VAE encoder), a diffusion module, an alignment module to incorporate the extracted LQ features with the noisy latent of the diffusion model, a text embedding extraction module (*i.e.*, a text encoder [28]) and a HQ image reconstruction module (*i.e.*, a VAE decoder). We unify the VAE encoder, alignment module, and diffusion model into a trainable framework while keeping the other components frozen due to the VAE decoder’s strong priors for reconstructing HQ images and the text encoder’s robust text-

image alignment capabilities. To connect LQ features extracted from VAE encoder with noisy latent, we first only pre-train the alignment module, while fixing the VAE encoder and the diffusion model. Then we jointly fine-tune the VAE encoder, the alignment module, and the diffusion model, in order to facilitate these three modules adapting to each other and leveraging their interplays. The fine-tuned VAE encoder is denoted as LQ encoder in Figure 2.

The proposed method is optimized by:

$$L = \left\| \epsilon - \hat{\epsilon}_\theta(\sqrt{\bar{\alpha}_t}x_0^{HQ} + \sqrt{1 - \bar{\alpha}_t}\epsilon, f^{LQ}, c, t) \right\|_1, \quad (3)$$

where  $\|\cdot\|_1$  is the L1 normalization,  $\epsilon$  is sampled from the standard normal distribution  $\mathcal{N}(0, \mathbf{I})$ ,  $x_0^{HQ}$  is generated from the HQ image by the pre-trained VAE encoder,  $\hat{\epsilon}_\theta$ ,  $\bar{\alpha}_t$ ,  $c$ , and  $t$  are defined the same as those in (2).

## 4. Experimental Results

In this section, we first describe the datasets and implementation details of the proposed method. Then we evaluate our approach against state-of-the-art ones using publicly available benchmark datasets. More experimental results are included in the supplemental material.

### 4.1. Datasets and implementation details

**Training dataset.** We collect a training dataset of high-resolution images from LSDIR [17], DIV2K [1], Flickr2K [20], DIV8K [7], and 10,000 face images from FFHQ [12]. We generate LQ images following the same configuration as [43]. Similar to [44], we use the LLAVA [22] to generate textual descriptions for each image.

**Synthetic test datasets.** Similar to DASR [18], we employ different levels of degradations (D-level) to synthesize degraded validation sets of DIV2K [1] and LSDIR [17].

**Real-world test datasets.** To evaluate our approach in real scenarios, we first test on the dataset of RealPhoto60 [44]. We then collect a dataset, named RealDeg, of 238 images including old photographs, classic film stills, and social media images to evaluate our method across diverse degradation types. More details are included in the supplemental material.

**Implementation details.** We choose the base model of SDXL [26] as our diffusion model and use its VAE encoder as our LQ encoder. We train the proposed method using two A800 GPUs and adopt the AdamW optimizer [24] with default parameters. We crop images into patches of  $512 \times 512$  pixels during training and set the batch size as 256. We first pre-train the proposed alignment module for 6,000 iterations with an initial learning rate of  $5 \times 10^{-5}$ . We then fine-tune the whole network including the LQ encoder, the alignment module, and the diffusion model in an end-to-end manner for 40,000 iterations. During the fine-tuning

Table 1. Quantitative comparison with state-of-the-art methods on the datasets of DIV2K-Val [1] and LSDIR-Val [17]. ‘Level I’, ‘Level II’, and ‘Level III’ denote the datasets with mild, medium, and severe degradations, respectively. The best and second performances are marked in red and blue, respectively.

D-Level	Methods	DIV2K-Val [1]					LSDIR-Val [17]				
		PSNR (dB) $\uparrow$	SSIM $\uparrow$	LPIPS $\downarrow$	MUSIQ $\uparrow$	CLIPQA+ $\uparrow$	PSNR (dB) $\uparrow$	SSIM $\uparrow$	LPIPS $\downarrow$	MUSIQ $\uparrow$	CLIPQA+ $\uparrow$
Level-I	Real-ESRGAN [40]	26.64	0.7737	0.1964	62.38	0.4649	23.47	0.7102	0.2008	69.23	0.5378
	BSRGAN [46]	27.63	0.7897	0.2038	61.81	0.4588	24.42	0.7292	0.2167	66.21	0.5037
	StableSR [38]	24.71	0.7131	0.2393	65.55	0.5156	21.57	0.6233	0.2509	70.52	0.6004
	DiffBIR [21]	24.60	0.6595	0.2496	66.23	0.5407	21.75	0.5837	0.2677	68.96	0.5693
	PASD [43]	25.31	0.6995	0.2370	64.57	0.4764	22.16	0.6105	0.2582	68.90	0.5221
	SeeSR [41]	25.08	0.6967	0.2263	66.48	0.5336	22.68	0.6423	0.2262	70.94	0.5815
	DreamClear [2]	23.76	0.6574	0.2259	66.15	0.5478	20.08	0.5493	0.2619	70.81	0.6182
	SUPIR [44]	25.09	0.7010	0.2139	65.49	0.5202	21.58	0.5961	0.2521	71.10	0.6118
	Ours	24.29	0.6668	0.2187	66.53	0.5432	21.20	0.5760	0.2264	71.25	0.6253
Level-II	Real-ESRGAN [40]	25.49	0.7274	0.2309	61.84	0.4719	22.47	0.6567	0.2342	69.14	0.5456
	BSRGAN [46]	26.42	0.7402	0.2465	60.00	0.4483	23.35	0.6682	0.2641	64.17	0.4858
	StableSR [38]	24.26	0.6771	0.2590	64.76	0.5057	21.58	0.5946	0.2802	69.57	0.5667
	DiffBIR [21]	24.42	0.6441	0.2708	64.83	0.5246	21.63	0.5672	0.2853	67.61	0.5555
	PASD [43]	24.89	0.6764	0.2502	64.45	0.4718	21.85	0.5846	0.2737	68.53	0.5131
	SeeSR [41]	24.65	0.6734	0.2428	66.09	0.5226	22.00	0.6026	0.2469	70.91	0.5837
	DreamClear [2]	23.39	0.6330	0.2518	64.96	0.5295	19.74	0.5191	0.2910	70.41	0.6072
	SUPIR [44]	24.42	0.6703	0.2432	65.58	0.5202	21.30	0.5713	0.2733	70.59	0.5998
	Ours	23.80	0.6413	0.2407	66.42	0.5460	20.88	0.5493	0.2469	71.15	0.6219
Level-III	Real-ESRGAN [40]	22.81	0.6288	0.3535	60.11	0.4637	20.13	0.5374	0.3650	67.02	0.5275
	BSRGAN [46]	23.45	0.6281	0.3462	62.41	0.4838	20.75	0.5358	0.3667	67.41	0.5363
	StableSR [38]	23.34	0.6277	0.3559	57.89	0.4124	20.55	0.5195	0.3716	64.31	0.4859
	DiffBIR [21]	23.42	0.5992	0.3676	58.86	0.5154	20.53	0.4809	0.3951	62.23	0.5148
	PASD [43]	22.58	0.5985	0.3646	63.08	0.4815	20.03	0.4974	0.3769	67.43	0.5092
	SeeSR [41]	22.58	0.5944	0.3278	65.82	0.5106	20.16	0.5046	0.3437	69.35	0.5444
	DreamClear [2]	21.82	0.5510	0.3336	62.59	0.4914	18.46	0.4341	0.3831	68.64	0.5757
	SUPIR [44]	21.90	0.5611	0.3172	65.46	0.5134	19.17	0.4650	0.3488	70.16	0.5917
	Ours	21.77	0.5662	0.3080	66.28	0.5275	18.92	0.4568	0.3170	71.37	0.6067

stage, the learning rate for the LQ encoder and other network components are initialized as  $5 \times 10^{-6}$  and  $10^{-5}$ , respectively. The learning rates are updated using the Cosine Annealing scheme [23]. To further enhance the controllability of our proposed method, we employ an image descriptions dropout operation in training to enable classifier-free guidance (CFG) [8]. We empirically set the image descriptions dropout ratio to 20% during training. For inference of FaithDiff, we adopt Euler scheduler [13] with 20 sampling steps and set CFG guidance scale as 5.

## 4.2. Comparisons with the state of the art

We compare our approach with state-of-the-art image SR methods including GAN-based methods (*i.e.*, Real-ESRGAN [40] and BSRGAN [46]) and diffusion-based methods (*i.e.*, StableSR [38], DiffBIR [21], PASD [43], DreamClear [2], and SUPIR [44]). We use PSNR, SSIM and perceptual-oriented metrics (*i.e.*, LPIPS [48], MUSIQ [14], and CLIPQA+ [37]) to evaluate the fidelity and quality of restored images.

**Evaluations on the synthetic datasets.** We first evaluate our approach on the datasets of DIV2K [1] and LSDIR [17]. Table 1 shows the quantitative results. Although GAN-based methods [40, 46] perform best in terms of PSNR and SSIM metrics, they exhibit poor performance in terms of MUSIQ [14] and CLIPQA+ [37] metrics. The proposed approach outperforms competing meth-

ods [2, 21, 38, 40, 41, 43, 44, 46] in terms of the perceptual-oriented metrics. Note that our method clearly improves the results, especially in the challenging cases of severe degradations, which demonstrates the effectiveness of our approach.

Figure 3 shows visual comparisons on an LQ images with severe degradations from LSDIR [17]. The results generated by GAN-based methods [40] exhibit perceptually unpleasant artifacts as shown in Figure 3(b). Existing diffusion-based methods [21, 38, 41, 44], however, also do not recover satisfying results. The method [38] that directly injects LQ input into the diffusion process generates over-smoothed regions, as shown in Figure 3(c), as frozen generative priors are difficult to align well with LQ input, which limits the powerful generative capability. Although the methods [21, 41, 44] propose to extract degradation-robust features from LQ inputs, any mistake in the LQ features can mislead the diffusion process to generate inaccurate results (*e.g.*, severe artifacts obtained in Figure 3(f) and incorrect structures generated in Figure 3(d) and (g)). In contrast, by unleashing the diffusion prior and jointly optimizing it with the encoder, our approach yields more realistic image with faithful structural details (*e.g.*, the restored feathers of a bird in Figure 3(h)) that are consistent with the ground truth as shown in Figure 3(e).

**Evaluations on the real-world datasets.** We further evaluate the proposed method on real-world scenarios. As high-

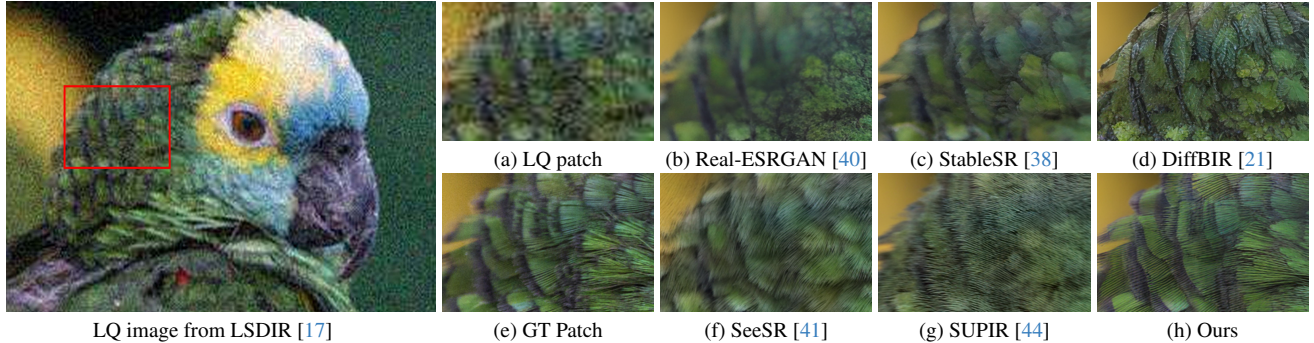


Figure 3. Image SR result ( $\times 4$ ) on the synthetic benchmark. The restored image by GAN-based methods [40] exhibits perceptually unpleasant artifacts in (b). Existing diffusion-based methods [21, 38, 41, 44] over-smooth the details in (c) or generate incorrect structures in (d) and (f)-(g). In contrast, the proposed method recovers much clearer images with faithful structures in (h).

Table 2. Quantitative comparison with state-of-the-art methods on real-world benchmarks. The best and second performances are marked in red and blue, respectively.

Benchmarks	Metrics	Real-ESRGAN [40]	BSRGAN [46]	StabeSR [38]	DiffBIR [21]	PASD [43]	SeeSR [41]	DreamClear [2]	SUPIR [44]	Ours
RealPhoto60 [44]	MUSIQ $\uparrow$	59.29	45.46	57.89	63.67	64.53	<b>70.80</b>	70.46	70.26	<b>72.74</b>
	CLIPQA+ $\uparrow$	0.4389	0.3397	0.4214	0.4935	0.4786	<b>0.5691</b>	0.5273	0.5528	<b>0.5932</b>
RealDeg	MUSIQ $\uparrow$	52.64	52.08	53.53	58.22	47.31	<b>60.10</b>	56.67	51.50	<b>61.24</b>
	CLIPQA+ $\uparrow$	0.3396	0.3520	0.3669	0.4258	0.3137	<b>0.4315</b>	0.4105	0.3468	<b>0.4327</b>

Table 3. Recognition results on the dataset of Occluded RoadText 2024 [35] (OCR recognition). The best and second performances are highlighted in red and blue, respectively.

Metrics	GT	LQ	Real-ESRGAN [40]	BSRGAN [46]	StableSR [38]	DiffBIR [21]	PASD [43]	SeeSR [41]	DreamClear [2]	SUPIR [44]	Ours
Precision	52.72%	7.54%	13.19%	12.04%	19.87%	26.21%	24.32%	30.07%	22.45%	<b>31.78%</b>	<b>36.45%</b>
Recall	56.67%	7.59%	13.68%	12.33%	20.31%	27.90%	25.14%	33.09%	23.50%	<b>41.57%</b>	<b>46.74%</b>

resolution images are not available, we use non-reference metrics (*i.e.*, MUSIQ [14] and CLIPQA+ [37]) to evaluate the quality of restored images in Table 2, where the proposed approach achieves the best performance, increasing MUSIQ [14] by at least 1.14.

Figure 4 shows one example from RealPhoto60 [44] and two examples from the RealDeg dataset. The proposed method generates more realistic images with better fine-scale structures and details (Figure 4(h)).

**Run-time comparison.** Benefiting from unleashing the diffusion prior and the alignment module, our approach does not need adaptors like ControlNet [47] to steer the diffusion process with LQ features, which significantly improve our efficiency. We further benchmark the run-time for the diffusion process of existing diffusion-based image SR methods and our approach on 10 images with the size of  $1024 \times 1024$  pixels in Table 4. All methods are tested on a machine with an A800 GPU. As shown in Tables 1-4, our proposed method is more efficient with better image quality.

### 4.3. Real-world OCR recognition

To further examine whether the proposed method generates faithful structures, we provide evaluation results on the OCR detection accuracy of the restored images. We select 200 images from ICDAR 2024 Occluded RoadText

Table 4. Run-time performance of diffusion-based SR methods for the diffusion process. All methods are tested on a machine with an A800 GPU. The best and second performances are highlighted in red and blue, respectively.

	DiffBIR [21]	PASD [43]	SeeSR [41]	DreamClear [41]	SUPIR [44]	Ours
Inference Step	50	20	50	50	50	20
Running Time (s)	46.81	<b>7.31</b>	10.31	7.58	11.44	<b>2.55</b>

dataset [35] and generate LQ images with severe degradations using the same method as described in Section 4.1. For OCR recognition, we use the robust visual backbone PaddleOCR v3 [16] to evaluate on the restored images by various SR methods. Table 3 shows that the OCR recognition accuracy of our restored images is better, indicating that our method is capable of effectively restoring reliable structural information.

## 5. Analysis and Discussion

### 5.1. Effectiveness of the alignment module

The alignment module is proposed to adaptively explore useful information from LQ features to facilitate the progressive diffusion process for faithful HQ image reconstruction. To demonstrate the effectiveness of our alignment module, we compare with a baseline method that removes the alignment module (Ours<sub>w/o Align</sub> for short). To leverage LQ features to guide the diffusion process, we respectively

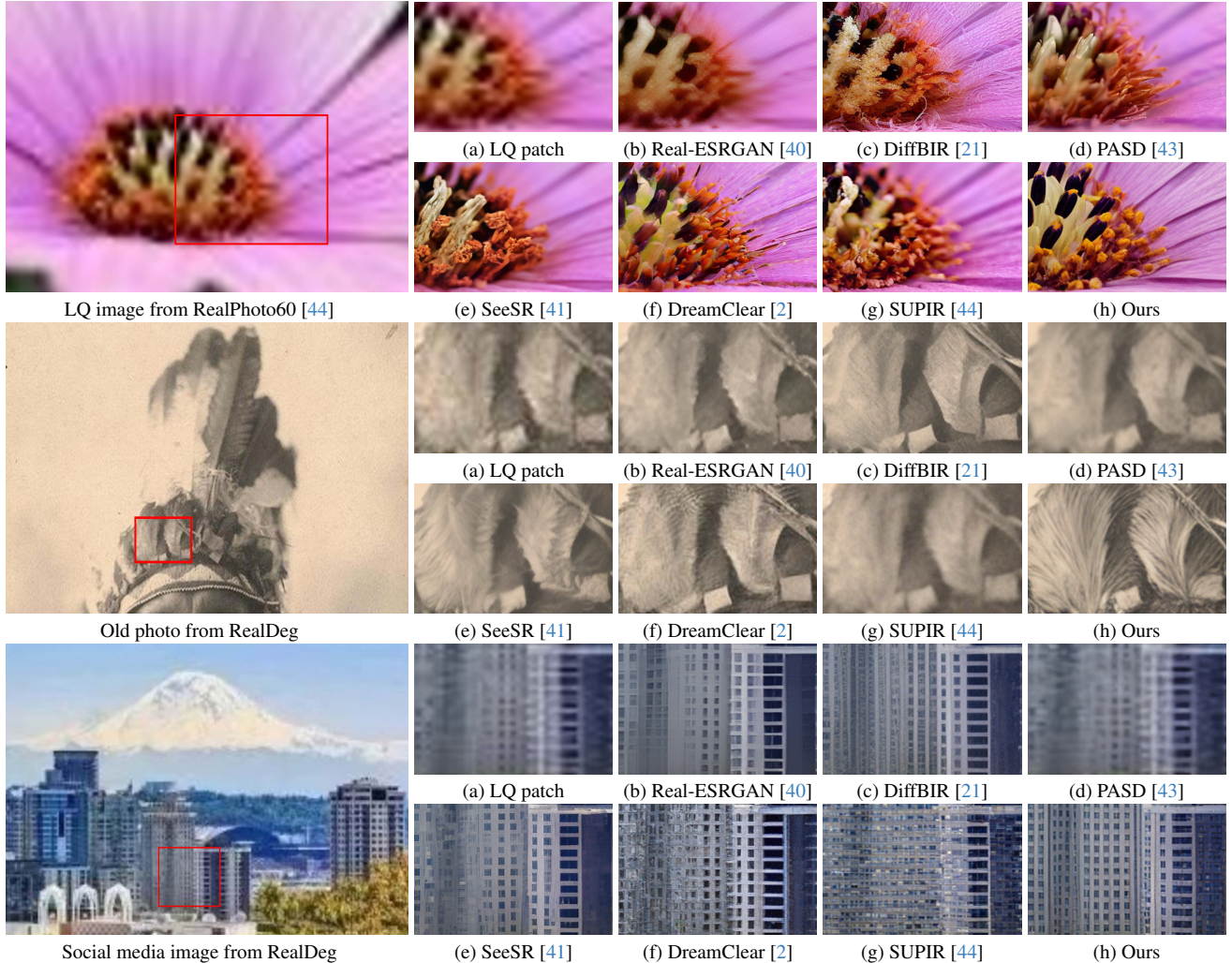


Figure 4. Image SR result ( $\times 2$ ) on the real-world benchmarks. Compared to competing methods, our approach generates more realistic images with fine-scale structures and details.

apply one convolutional layer on the noisy latent as well as the LQ features and then add their results together. The quantitative results in Table 5 show that the MUSIQ of our approach is 6.07 higher than the baseline method on the RealPhoto60 dataset. The comparison results illustrate that the proposed alignment module is more effective in capturing useful information from LQ features to facilitate the diffusion process.

To further analyze the effect of pre-training the alignment module, we compare our approach with a baseline that does not pre-train the alignment module but directly trains it together with the whole network ( $\text{Ours}_{\text{w/o Pre-train align}}$  for short). The results in Table 5 demonstrate the effectiveness of pre-training the alignment module, which is more effective in exploiting useful features from LQ features and incorporating them with the noisy latent of the diffusion model, increasing the MUSIQ by 2.98 on the RealPhoto60 dataset [44].

We additionally investigate whether it is necessary to use the visual features from the penultimate layer of the LQ encoder instead of those from the last layer. To this end, we further compare with a baseline that replaces the LQ features with the visual features of the last layer of the LQ encoder ( $\text{Ours}_{\text{w/ Last feats}}$  for short). As Table 5 shows, our approach performs better than the baseline, decreasing the LPIPS by 0.0222 on the DIV2K-Val [1] dataset and increasing the MUSIQ by 2.69 on the RealPhoto60 [44] dataset. The comparison results demonstrate that the features extracted from the penultimate layer of the VAE encoder can effectively capture more useful information.

## 5.2. Effectiveness of unified feature optimization

To demonstrate the effectiveness of the proposed unified feature optimization strategy, we compare with baseline methods that respectively fix the diffusion model (FT EN & Fix DM for short), fix the encoder (Fix EN & FT DM



Figure 6. Visualization of DAAMs [33] for ‘bottles’. (b)-(d) are DAAMs for PASD [43], SeeSR [41], and our method.

Table 5. Effectiveness of the proposed alignment module. All methods are trained using the same settings as the proposed method for fair comparison.

	Alignment module	Pre-train alignment	Penultimate visual features	DIV2K-Val [1] LPIPS ↓	RealPhoto60 [44] MUSIQ ↑
Ours <sub>wo</sub> Align	✗	✓	✓	0.3199	66.67
Ours <sub>wo</sub> Pre-train align	✓	✗	✓	0.3244	69.76
Ours <sub>wo</sub> Last feats	✓	✓	✗	0.3302	70.05
Ours	✓	✓	✓	0.3080	72.74

Table 6. Effectiveness of unified feature optimization. All methods are trained using the same settings for fair comparison. SP denotes separately fine-tuning encoder and diffusion model.

	Encoder (EN)		Diffusion model (DM)		DIV2K-Val [1] LPIPS ↓	RealPhoto60 [44] MUSIQ ↑
	Fix	Fine-tune (FT)	Fix	Fine-tune (FT)		
FT EN & Fix DM	✗	✓	✗	✗	0.3370	69.66
Fix EN & FT DM	✓	✗	✓	✓	0.3302	71.11
FT EN & DM (SP)	✗	✓	✗	✓	0.3261	69.94
Ours	✗	✓	✗	✓	0.3080	72.74

for short), as well as separately fine-tune the encoder and diffusion model (FT EN & DM (SP) for short). Note that for FT EN & Fix DM, we use ControlNet [47] with the spatial feature transfer block (SFT) [44] to make the LQ features suitable for guiding the diffusion process. As shown in Table 6, the proposed approach outperforms all baseline methods, increasing the MUSIQ by at least 1.63 on the RealPhoto60 [44] dataset. This demonstrates the importance of jointly optimizing the encoder and the diffusion model, which can benefit from their interplay.

Figure 5 shows a visual comparison on an image from DIV2K-Val [1] with severe degradations. The main structures generated by FT EN & Fix DM are inconsistent with the ground truth, cf. the ‘windows’ obtained by FT EN & Fix DM in Figure 5(b) vs. the characters ‘MAER’ of the GT in Figure 5(d). As the diffusion model is pre-trained on HQ images, any mistakes in the LQ features can mislead the diffusion model into generating incorrect image structures. The comparison results in Figure 5 show that unleashing the diffusion model is able to improve the performance, but only yields faithful results when jointly optimized with the encoder. This demonstrates that the proposed unified feature optimization strategy is able to benefit from the interplay of the encoder and the diffusion model, resulting in high-fidelity results, as shown in Figure 5(f).

### 5.3. Visualization of DAAMs

We visualize diffusion attentive attribution maps (DAAMs) [33] of some state-of-the-art diffusion-based methods and our approach in Figure 6. Given an LQ image and the text ‘bottle’ from the prompt ‘An image of an outdoor market with a lot of food and bottles’, we upscale and aggregate

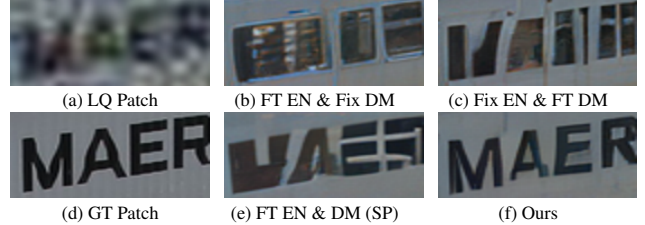


Figure 5. Effectiveness of the unified feature optimization on image SR ( $\times 4$ ). Using unify optimization strategy is able to generate the results with clearer structural details.

cross-attention maps in LDM during diffusion process to fetch DAAMs [33]. For LQ images with severe degradation in Figure 6(a), it is hard to extract accurate structural information, thus existing ControlNet-based methods [41, 43] yield weaker responses when calculating the similarity between LQ features and text embeddings (Figure 6(b)-(c)). This hinders the activation of pre-trained diffusion priors and the restoration of faithful results as shown in Figure 6(e)-(f). In contrast, our proposed approach unleashes diffusion priors and jointly optimizes the encoder and diffusion model to enable them to benefit from each other. Thus, our method can effectively capture more useful information from LQ images, leading to a more plausible DAAM in Figure 6(d) and more faithful results in Figure 6(g).

## 6. Conclusion

In this paper, we propose an effective image SR method, named FaithDiff, which unleashes diffusion priors to better harness the powerful representation ability of LDM. We show that unleashing diffusion priors is more effective in exploring useful information from degraded inputs and restoring faithful results. We further develop an alignment module that effectively incorporates the features extracted by the encoder with the noisy latent of the diffusion model. Taking all the components into one trainable network, we jointly optimize the encoder, alignment module, and the diffusion model. This unified optimization strategy enables the encoder to provide useful features that coincide with the diffusion process, while the latent diffusion model can further restore these features. Benefiting from their interplay, the entire network can effectively distinguish between degradation effects and inherent structural information, resulting in high-quality restoration. Extensive experiments on synthetic and real-world benchmarks demonstrate that FaithDiff outperforms state-of-the-art methods in terms of structural fidelity and visual quality.

## References

- [1] Eirikur Agustsson and Radu Timofte. Ntire 2017 challenge on single image super-resolution: Dataset and study. In *CVPR Workshops*, 2017. 4, 5, 7, 8
- [2] Yang Ai, Xiaoqiang Zhou, Huaibo Huang, Xiaotian Han, Zhengyu Chen, Quanzeng You, and Hongxia Yang. Dreamclear: High-capacity real-world image restoration with privacy-safe dataset curation. In *NeurIPS*, 2024. 5, 6, 7
- [3] Kelvin CK Chan, Xintao Wang, Xiangyu Xu, Jinwei Gu, and Chen Change Loy. Glean: Generative latent bank for large-factor image super-resolution. In *CVPR*, 2021. 1
- [4] Chaofeng Chen, Xinyu Shi, Yipeng Qin, Xiaoming Li, Xiaoguang Han, Tao Yang, and Shihui Guo. Real-world blind super-resolution via feature matching with implicit high-resolution priors. In *ACM MM*, 2022. 1, 2
- [5] Junsong Chen, Jincheng Yu, Chongjian Ge, Lewei Yao, Enze Xie, Yue Wu, Zhongdao Wang, James Kwok, Ping Luo, Huchuan Lu, et al. Pixart- $\alpha$ : Fast training of diffusion transformer for photorealistic text-to-image synthesis. In *ICLR*, 2024. 1, 2
- [6] Jinjin Gu, Hannan Lu, Wangmeng Zuo, and Chao Dong. Blind super-resolution with iterative kernel correction. In *CVPR*, 2019. 2
- [7] Shuhang Gu, Andreas Lugmayr, Martin Danelljan, Manuel Fritsche, Julien Lamour, and Radu Timofte. Div8k: Diverse 8k resolution image dataset. In *ICCV Workshops*, 2019. 4
- [8] Jonathan Ho and Tim Salimans. Classifier-free diffusion guidance. *arXiv preprint arXiv:2207.12598*, 2022. 5
- [9] Jonathan Ho, Ajay Jain, and Pieter Abbeel. Denoising diffusion probabilistic models. In *NeurIPS*, 2020. 2
- [10] Li Hu, Xin Gao, Peng Zhang, Ke Sun, Bang Zhang, and Liefeng Bo. Animate anyone: Consistent and controllable image-to-video synthesis for character animation. In *CVPR*, 2024. 3
- [11] Yan Huang, Shang Li, Liang Wang, Tieniu Tan, et al. Unfolding the alternating optimization for blind super resolution. In *NeurIPS*, 2020. 2
- [12] Tero Karras, Samuli Laine, and Timo Aila. A style-based generator architecture for generative adversarial networks. In *CVPR*, 2019. 4
- [13] Tero Karras, Miika Aittala, Timo Aila, and Samuli Laine. Elucidating the design space of diffusion-based generative models. In *NeurIPS*, 2022. 5
- [14] Junjie Ke, Qifei Wang, Yilin Wang, Peyman Milanfar, and Feng Yang. Musiq: Multi-scale image quality transformer. In *CVPR*, 2021. 5, 6
- [15] Diederik P Kingma. Auto-encoding variational bayes. In *ICLR*, 2014. 3
- [16] Chenxia Li, Weiwei Liu, Ruoyu Guo, Xiaoting Yin, Kaitao Jiang, Yongkun Du, Yuning Du, Lingfeng Zhu, Baohua Lai, Xiaoguang Hu, et al. Pp-ocrv3: More attempts for the improvement of ultra lightweight ocr system. *arXiv preprint arXiv:2206.03001*, 2022. 6
- [17] Yawei Li, Kai Zhang, Jingyun Liang, Jiezhang Cao, Ce Liu, Rui Gong, Yulun Zhang, Hao Tang, Yun Liu, Denis Deman-dolx, et al. Lsdnet: A large scale dataset for image restoration. In *CVPR*, 2023. 4, 5, 6
- [18] Jie Liang, Hui Zeng, and Lei Zhang. Efficient and degradation-adaptive network for real-world image super-resolution. In *ECCV*, 2022. 2, 4
- [19] Jie Liang, Hui Zeng, and Lei Zhang. Details or artifacts: A locally discriminative learning approach to realistic image super-resolution. In *CVPR*, 2022. 1, 2
- [20] Bee Lim, Sanghyun Son, Heewon Kim, Seungjun Nah, and Kyoung Mu Lee. Enhanced deep residual networks for single image super-resolution. In *CVPR Workshops*, 2017. 4
- [21] Xinqi Lin, Jingwen He, Ziyang Chen, Zhaoyang Lyu, Bo Dai, Fanghua Yu, Wanli Ouyang, Yu Qiao, and Chao Dong. Diffbir: Towards blind image restoration with generative diffusion prior. *arXiv preprint arXiv:2308.15070*, 2023. 1, 2, 3, 5, 6, 7
- [22] Haotian Liu, Chunyuan Li, Qingyang Wu, and Yong Jae Lee. Visual instruction tuning. In *NeurIPS*, 2024. 4
- [23] Ilya Loshchilov and Frank Hutter. Sgdr: Stochastic gradient descent with warm restarts. In *ICLR*, 2017. 5
- [24] Ilya Loshchilov and Frank Hutter. Decoupled weight decay regularization. In *ICLR*, 2019. 4
- [25] Chong Mou, Xintao Wang, Liangbin Xie, Yanze Wu, Jian Zhang, Zhongang Qi, and Ying Shan. T2i-adapter: Learning adapters to dig out more controllable ability for text-to-image diffusion models. In *AAAI*, 2024. 2
- [26] Dustin Podell, Zion English, Kyle Lacey, Andreas Blattmann, Tim Dockhorn, Jonas Müller, Joe Penna, and Robin Rombach. Sdxl: Improving latent diffusion models for high-resolution image synthesis. In *ICLR*, 2024. 1, 2, 4
- [27] Yunpeng Qu, Kun Yuan, Kai Zhao, Qizhi Xie, Jinhua Hao, Ming Sun, and Chao Zhou. Xpsr: Cross-modal priors for diffusion-based image super-resolution. In *ECCV*, 2024. 1, 2
- [28] Alec Radford, Jong Wook Kim, Chris Hallacy, Aditya Ramesh, Gabriel Goh, Sandhini Agarwal, Girish Sastry, Amanda Askell, Pamela Mishkin, Jack Clark, et al. Learning transferable visual models from natural language supervision. In *ICML*, 2021. 4
- [29] Aditya Ramesh, Prafulla Dhariwal, Alex Nichol, Casey Chu, and Mark Chen. Hierarchical text-conditional image generation with clip latents. *arXiv preprint arXiv:2204.06125*, 2022. 2
- [30] Robin Rombach, Andreas Blattmann, Dominik Lorenz, Patrick Esser, and Björn Ommer. High-resolution image synthesis with latent diffusion models. In *CVPR*, 2022. 2
- [31] Robin Rombach, Andreas Blattmann, Dominik Lorenz, Patrick Esser, and Björn Ommer. High-resolution image synthesis with latent diffusion models. In *CVPR*, 2022. 1, 2
- [32] Chitwan Saharia, William Chan, Saurabh Saxena, Lala Li, Jay Whang, Emily L Denton, Kamyar Ghasemipour, Raphael Gontijo Lopes, Burcu Karagol Ayan, Tim Salimans, et al. Photorealistic text-to-image diffusion models with deep language understanding. In *NeurIPS*, 2022. 1, 2
- [33] Raphael Tang, Linqing Liu, Akshat Pandey, Zhiying Jiang, Gefei Yang, Karun Kumar, Pontus Stenetorp, Jimmy Lin, and Ferhan Ture. What the daam: Interpreting stable diffusion using cross attention. *arXiv preprint arXiv:2210.04885*, 2022. 8

- [34] Linrui Tian, Qi Wang, Bang Zhang, and Liefeng Bo. Emo: Emote portrait alive - generating expressive portrait videos with audio2video diffusion model under weak conditions. In *ECCV*, 2024. 3
- [35] George Tom, Minesh Mathew, Ajoy Mondal, Dimosthenis Karatzas, C. V. Jawahar, and Jerod Weinman. Icdar2024 challenge on occluded roadtext. In *ICDAR2024 Workshops*, 2024. 6
- [36] A Vaswani. Attention is all you need. In *NeurIPS*, 2017. 4
- [37] Jianyi Wang, Kelvin CK Chan, and Chen Change Loy. Exploring clip for assessing the look and feel of images. In *AAAI*, 2023. 5, 6
- [38] Jianyi Wang, Zongsheng Yue, Shangchen Zhou, Kelvin CK Chan, and Chen Change Loy. Exploiting diffusion prior for real-world image super-resolution. *IJCV*, 2024. 2, 5, 6
- [39] Xintao Wang, Yu Li, Honglun Zhang, and Ying Shan. Towards real-world blind face restoration with generative facial prior. In *CVPR*, 2021. 1
- [40] Xintao Wang, Liangbin Xie, Chao Dong, and Ying Shan. Real-esrgan: Training real-world blind super-resolution with pure synthetic data. In *CVPR*, 2021. 1, 2, 5, 6, 7
- [41] Rongyuan Wu, Tao Yang, Lingchen Sun, Zhengqiang Zhang, Shuai Li, and Lei Zhang. Seesr: Towards semantics-aware real-world image super-resolution. In *CVPR*, 2024. 2, 5, 6, 7, 8
- [42] Liangbin Xie, Xintao Wang, Xiangyu Chen, Gen Li, Ying Shan, Jiantao Zhou, and Chao Dong. Desra: detect and delete the artifacts of gan-based real-world super-resolution models. In *ICML*, 2023. 1, 2
- [43] Tao Yang, Rongyuan Wu, Peiran Ren, Xuansong Xie, and Lei Zhang. Pixel-aware stable diffusion for realistic image super-resolution and personalized stylization. In *ECCV*, 2024. 1, 2, 4, 5, 6, 7, 8
- [44] Fanghua Yu, Jinjin Gu, Zheyuan Li, Jinfan Hu, Xiangtao Kong, Xintao Wang, Jingwen He, Yu Qiao, and Chao Dong. Scaling up to excellence: Practicing model scaling for photo-realistic image restoration in the wild. In *CVPR*, 2024. 1, 2, 3, 4, 5, 6, 7, 8
- [45] Kai Zhang, Wangmeng Zuo, and Lei Zhang. Learning a single convolutional super-resolution network for multiple degradations. In *CVPR*, 2018. 2
- [46] Kai Zhang, Jingyun Liang, Luc Van Gool, and Radu Timofte. Designing a practical degradation model for deep blind image super-resolution. In *CVPR*, 2021. 1, 2, 5, 6
- [47] Lvmin Zhang, Anyi Rao, and Maneesh Agrawala. Adding conditional control to text-to-image diffusion models. In *ICCV*, 2023. 2, 6, 8
- [48] Richard Zhang, Phillip Isola, Alexei A Efros, Eli Shechtman, and Oliver Wang. The unreasonable effectiveness of deep features as a perceptual metric. In *CVPR*, 2018. 5
- [49] Shangchen Zhou, Kelvin Chan, Chongyi Li, and Chen Change Loy. Towards robust blind face restoration with codebook lookup transformer. In *NeurIPS*, 2022. 1